Practical aspects of Kelvin probe force microscopy

H. O. Jacobs, H. F. Knapp, and A. Stemmer[a)]
Swiss Federal Institute of Technology, Nanotechnology Group, Institute of Robotics, ETH Center/CLA, CH-8092 Zurich, Switzerland

(Received 14 July 1998; accepted for publication 24 November 1998)

We discuss practical aspects of Kelvin probe force microscopy (KFM) which are important to obtain stable images of the electric surface potential distribution at high spatial resolution (<100 nm) and high potential sensitivity (<1 mV) on conducting and nonconducting samples. We compare metal-coated and semiconducting tips with respect to their suitability for KFM. Components of the metal coating can become detached during scanning, introducing sudden offset jumps in the potential maps (typically up to 350 mV between adjacent scan lines). However, *n*-doped silicon tips show no substantial tip alterations and, therefore, provide a stable reference during the experiment (offset jumps typically up to 40 mV between adjacent scan lines). These semiconducting tips must be electrically connected via contact pads. We use InGa and colloidal silver pads which are easily applied to the substrate supporting the cantilever and have a low enough differential contact resistance (350 Ω and 2.2 kΩ, respectively). Furthermore, we introduce a simple procedure to fine tune the feedback which detects the electric surface potential and show how the basic KFM setup has to be modified to gain access to the necessary control signals. © *1999 American Institute of Physics.* [S0034-6748(99)00303-2]

I. INTRODUCTION

In both semiconductor devices and biological samples, knowledge of the local electric potential distribution is of significant interest because it helps to link the specimen's observed function with its local structure and composition. For instance, junctions between different materials, locations of electric short circuits, and the distribution of the electric field intensity are all of major interest in semiconductor device design as well as failure analysis.

Both scanning tunneling microscopy (STM) and atomic force microscopy (AFM) have been modified to obtain high resolution maps of the electric surface potential distribution. Until now scanning tunneling potentiometry (STP)[1–3] is the only method which provides near-atomic resolution. However, the application of STP is limited because most active devices are surrounded by an insulator. With the adaptation of the AFM to electric potential measurements[4,5] this major disadvantage was overcome, because the tip could now be kept close to the surface without the necessity of a tunneling current. In particular, variations of the Kelvin probe force microscope[6–8] (KFM) have evolved into reliable tools to characterize specimens ranging from semiconductor devices[9,10] to biological samples.[11,12]

All KFM microscopes use the same principle to measure the contact potential difference (CPD) between tip and sample surface: An alternating current (ac) voltage with adjustable direct current (dc) offset is applied between a conducting AFM tip and the sample electrode and the resulting electrostatic force is detected by a lock-in amplifier, and a feedback circuit controls the dc tip potential until the CPD is compensated (see also Fig. 1).

Although this potential measuring principle is identical for all KFM setups, the selected tips and the parameters of the feedback electronics determine whether high resolution and stable potential images are obtained or not. We report here about the advantage of using uncoated semiconducting tips compared to metal-coated ones, and describe a practical procedure for adjusting the feedback electronics to maintain optimum performance.

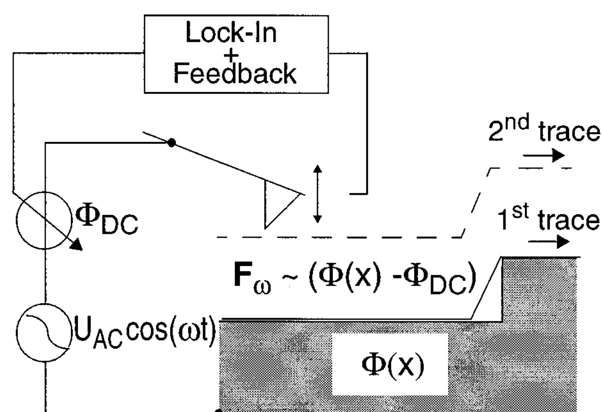

FIG. 1. KFM principle to measure the surface potential distribution. In the first trace (solid line) the topography of a single line is acquired using standard tapping mode (mechanical excitation of the cantilever). In the second trace (dashed line) this topography is retraced at a set lift height from the sample surface to detect the electric surface potential $\Phi(x)$. During this second trace the cantilever is no longer excited mechanically but electrically by applying the periodic voltage $U_{ac}\cos(\omega t)$ to the tip. The feedback then changes the dc tip potential Φ_{dc} until the ω component of the tip-force vanishes $[\Phi_{dc}=\Phi(x)]$.

[a)]Author to whom correspondence should be addressed; electronic mail: stemmer@ifr.mavt.ethz.ch

 © 1999 American Institute of Physics

Downloaded 20 Jan 2009 to 128.101.170.33. Redistribution subject to AIP license or copyright; see http://rsi.aip.org/rsi/copyright.jsp

II. INSTRUMENT SETUP

Our KFM microscope is based on a modified commercial AFM (NanoScope® IIIa Multimode™ with Extender™ Electronics Module, Digital Instruments USA) where topography and CPD are measured sequentially using the lift-mode technique to minimize cross talk (Fig. 1).[13] To this end, we first acquire the surface topography of a single line in TappingMode™ and then immediately retrace this topography over the same line at a set left height from the sample surface to measure the CPD. Images are obtained by repeating this procedure for each line along the slow-scan axis. The CPD is acquired using the standard KFM feedback loop provided by the Extender Electronics Module. All measurements are taken in air at ambient pressure and humidity. Under these conditions the actual value of the CPD is affected by contamination, oxide layers, or trapped surface charges.[6] The humidity plays an important role on charging effects on insulators. At low humidity (10% r.h.) trapped surface charges can be detected in the CPD image. such charging effects become less prominent at high humidity (80% r.h.).

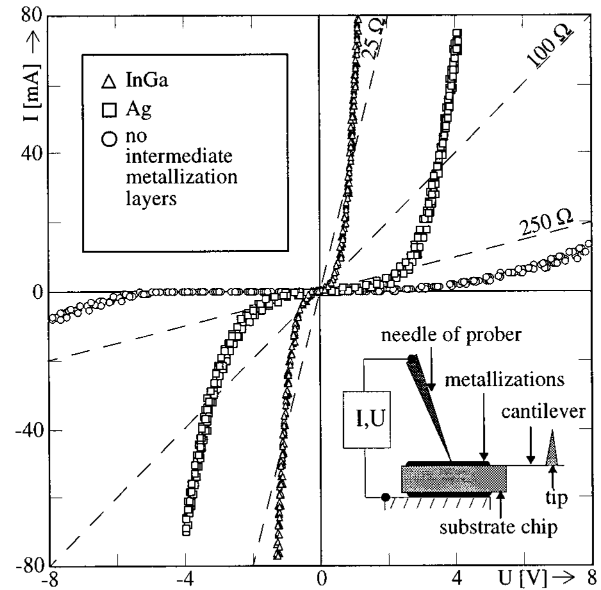

FIG. 2. Current-to-voltage characteristics of three different electric contacts to the *n*-type silicon cantilever substrate. Circles indicate the contact resistance when no intermediate contact metallization is present. With InGa (triangles) or silver paint (squares) contact pads the contact resistance is reduced to sufficiently small values for KFM applications. For comparison, the straight dashed reference lines show three different ohmic contacts.

III. TIP EFFECTS, PREPARATION, AND PERFORMANCE

In KFM the tip geometry is the most critical factor defining resolution and accuracy of the acquired potential maps: Long and slender, but slightly blunt tips, on cantilevers of minimal width and surface area are the best choice[14] if no guarding electrode covers the sides of the tip and the cantilever.[15] It is important to note that the measured CPD is always a weighted average, and all surface elements of the tip and the sample affect its value.[14]

Metal-coated AFM tips are most commonly used as they are commercially available and easy to produce. Unfortunately, the metal coats exhibit poor stability and the tip electrode often loses parts of its coating during scanning.[16] As a result, the tip electrode will act as an unstable reference since its surface potential distribution is changing during the measurement. To eliminate this possible source of error (detachment of parts of the metal coating), we use highly doped semiconducting tips which are electrically connected via a contact pad applied prior to the measurements.

To compare metal-coated tips with uncoated ones we modified commercially available Sb-doped silicon tapping-

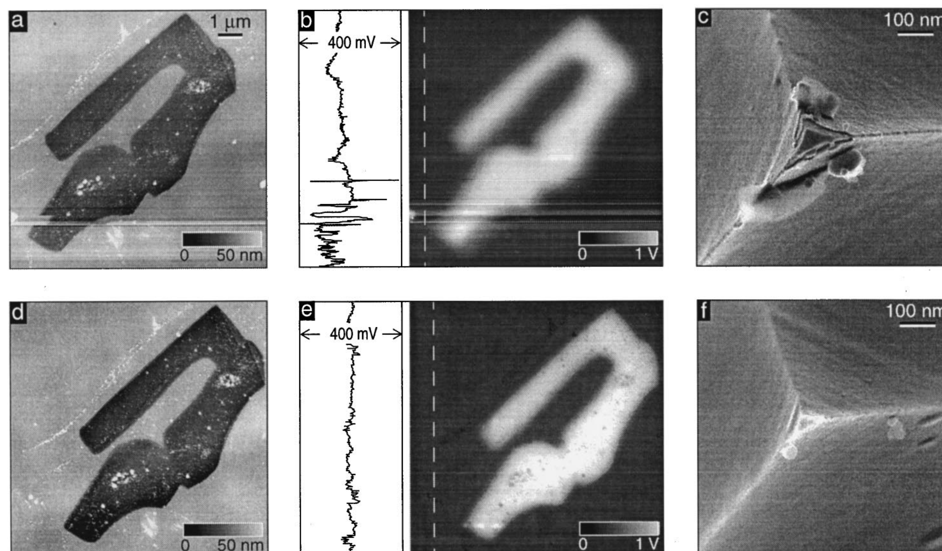

FIG. 3. Comparison of metal-coated tips vs semiconducting uncoated ones. The top row shows topography (a), CPD (b), and the metal-coated tip (c) after imaging the perforated metal film. The bottom row shows the same region of the sample but measured with an uncoated semiconducting tip (f). The potential fluctuations (b) and (e) which are measured along the slow scan axis (dashed line) are caused by alterations of the tip electrode. These alterations are generally larger for metal-coated tips.

Downloaded 20 Jan 2009 to 128.101.170.33. Redistribution subject to AIP license or copyright; see http://rsi.aip.org/rsi/copyright.jsp

mode tips (Nanosensors, Dr. O. Wolter GmbH, Germany) as described below. We found these probes preferable for KFM applications since the integrated tips are longer and the cantilevers have a smaller surface area compared to other commercially available ones. Tips were either metal-coated by sputtering 10 nm Pt onto the entire sensor including tip, cantilever, and substrate chip, or left uncoated but equipped with contact pads on both sides of the substrate chip. An electric contact pad to Sb-doped silicon is readily obtained by spreading and scratching InGa (InGa alloy, Johnson & Matthey AG, Zurich) onto the substrate of the tip. As the disposal of InGa is critical we also tried a fast-drying silver suspension (Silver Print, Provac AG, Liechtenstein). Figure 2 compares the InGa and ''silver paint'' contact pads (pad area $\sim$5.7 mm^2) with a direct contact where no intermediate conducting layer is present between the contact needle and the n-doped silicon substrate. For the shown current-to-voltage curves the differential contact resistance $(dI/dU)|_{U=0\ \mathrm{V}}$ is $\sim$350 Ω for InGa and $\sim$2.2 kΩ for silver paint and practically does not depend on the force exerted by the probe needle (see inset in Fig. 2). In contrast, the electrical characteristics in the case of the direct contact strongly depend on the force exerted by the probe needle. For low contact forces no electric contact is established, whereas at high contact forces the measured differential contact resistance was typically in between 400 kΩ and 2 MΩ.

In KFM the tip-sample capacitance and the contact resistance define the time delay between the actual tip potential and the compensating externally applied potential. For the used tips the total tip-sample capacitance is 0.6 fF at 15 nm tip-sample separation[14] and the time constant $\tau = R^*C$ becomes $\sim$1.3 ps for the silver paint contact. Since this time constant is much smaller than the periodicity of the ac driving voltage $1/f_r \approx 1/250\,\mathrm{kHz} = 4\ \mu\mathrm{s}$ (f_r=resonance frequency of the cantilever) the silver paint contact is sufficient for KFM applications and used in our experiments.

To obtain a test structure to compare the performance of metal-coated and uncoated semiconducting tips we fabricated a perforated metal film on a GaAs substrate following a published protocol.[13] To this end, we first spread 30% aqueous NaCl solution on the hydrophobic GaAs substrate surface, which was covered with a piece of rice paper to obtain an even distribution of the salt solution. The rice paper was removed once the salt solution had completely dried. After evaporation of 8 nm Pt–C the whole structure was rinsed with ultrapure water to dissolve the salt crystals and create the desired structure.

Figure 3 displays topography and CPD image of such a perforated Pt–C film taken with a metal-coated [Figs. 3(a) and 3(b)] and an uncoated semiconducting tip [Figs. 3(d) and 3(e)], respectively. In both potential images [Figs. 3(b) and 3(e)] the CPD shows sudden offset jumps along the vertical slow scan axis. However, for the uncoated semiconducting tip these offset jumps are typically up to 40 mV between adjacent scan lines, whereas for metal-coated ones offset jumps of up to 350 mV between adjacent scan lines are detected. The nature of these fluctuations are changes of the reference electrode, i.e., AFM tip, due to pick-up or loss of material [Figs. 3(c) and 3(f)] or charges. In the case of metal-coated tips, the large-scale fluctuations can be explained by substantial tip alterations due to abrasion of the metal coating as evidenced in Fig. 3(c).

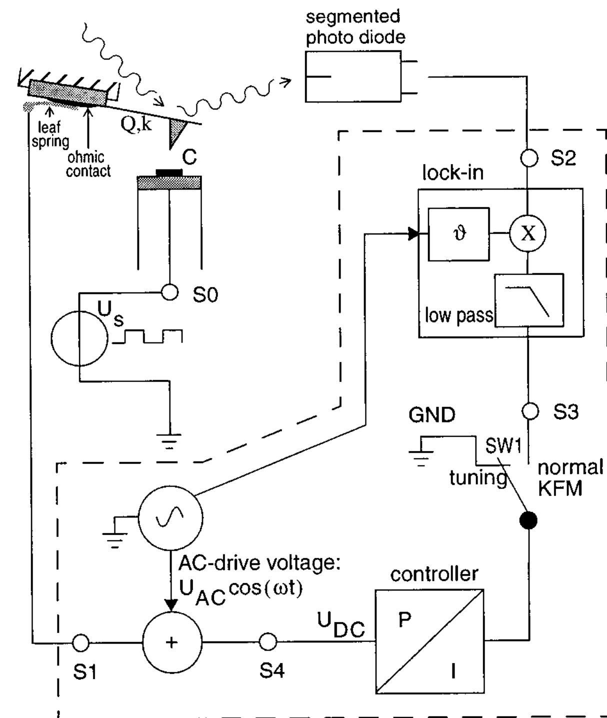

S1: $U_{DC} + U_{AC}\cos(\omega t)$

S2: $\frac{1}{2}\frac{Q}{k}\frac{\partial C}{\partial z}((U_{AC}\cos(\omega t - \varphi)) + (U_{DC} - U_s))^2$ $(\omega = \omega_r)$

$\frac{Q}{k}\frac{\partial C}{\partial z}U_{AC}(U_{DC} - U_s)\cos(\omega t + \varphi)$ (ω component)

S3: $\frac{1}{2}\frac{Q}{k}\frac{\partial C}{\partial z}U_{AC}(U_{DC} - U_s)\cos(\varphi - \vartheta)$ $(\varphi - \vartheta)_{opt} = 180°$

S4: U_{DC}

FIG. 4. Schematic of the KFM setup and all signals necessary to optimize the feedback. The square-wave voltage U_s is applied to the conductive sample during optimization. Phase ϑ is set by maximizing the output of the lock-in amplifier $S3$ when no feedback is present (open loop, $SW1$ switched to tuning). In closed loop ($SW1$ switched to normal KFM) the controller gains PI are fine tuned until the dc tip potential $S4$ tracks the square-wave voltage U_s. Symbol definitions: Q quality factor, k cantilever spring constant, C tip sample capacitance, φ phase shift, ω_r resonance frequency of the cantilever.

IV. FINE-TUNING THE FEEDBACK

In addition to optimizing the tip electrode, fine tuning the feedback is crucial for sensitive and stable potential measurements. Figure 4 shows a schematic circuit diagram of the KFM setup including all signals necessary to optimize the feedback. The electronics within the dashed line are located in the Extender™ Electronics Module. To this circuit we have added signal access points to (i) the output of the tip voltage, $S1$, (ii) the cantilever deflection signal, $S2$, (iii) the output of the lock-in amplifier, $S3$, and (iv) the output of the PI controller, $S4$. Furthermore, the switch $SW1$ was added to the input of the PI controller allowing us to turn off the feedback.

Downloaded 20 Jan 2009 to 128.101.170.33. Redistribution subject to AIP license or copyright; see http://rsi.aip.org/rsi/copyright.jsp

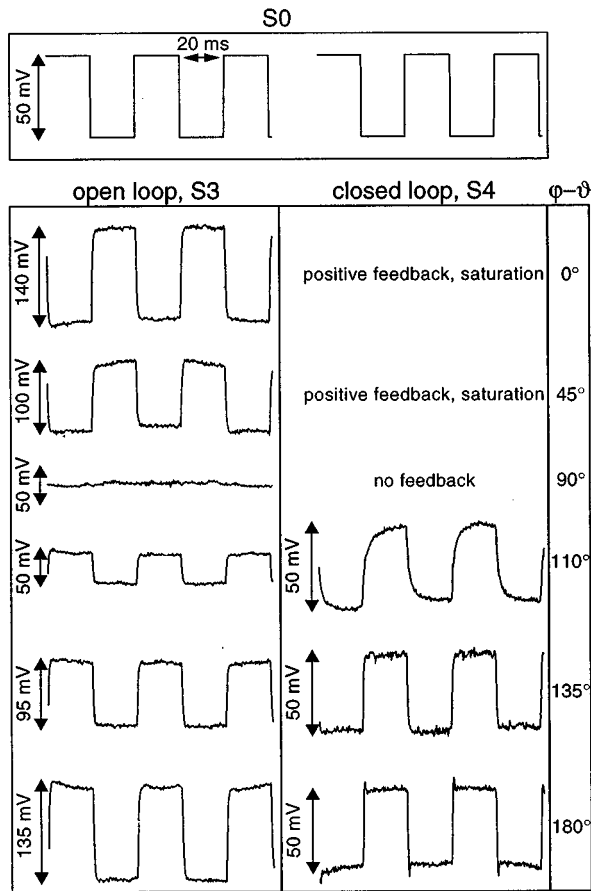

FIG. 5. Measured influence of the reference phase ϑ on the open-loop lock-in output signal $S3$ and the closed-loop dc tip potential $S4$. Generally $(\varphi-\vartheta)$ is unknown; a 90° phase difference $(\varphi-\vartheta)$ is indicated when the open-loop signal $S3$ becomes zero. By subtracting 90° from the corresponding ϑ value the correct reference phase ϑ is found, $S3$ is maximized, and highest sensitivity is achieved for the closed-loop dc tip potential $S4$ (CPD).

We found that the phase difference between the reference signal (used for the multiplication in the lock-in section) and the deflection signal of the cantilever carefully has to be set to the optimum value, i.e., 180° in our case, to achieve highest sensitivity. Besides the increased sensitivity, a phase jitter of the deflection signal becomes less important at 180°, which is not the case when working close to 90°.

The phase φ of the deflection signal (Fig. 4, $S2$) relative to the ac-drive voltage depends on the tip and the oscillation frequency, which is set to the cantilever's resonance to take advantage of the high Q factor at resonance. Hence, each time the tip is changed the phase of the reference, ϑ, must be adjusted to maximize the output of the lock-in amplifier ($S3$). However, only when the feedback loop is switched off ($SW1$ set to GND, Fig. 4), can the effect of the reference phase on the output of the lock-in be detected since in normal KFM operation ($SW1$ closed, Fig. 4) $S3$ is controlled to be zero.

To fine tune the feedback we apply an external square-wave voltage U_s to the sample surface (Fig. 4, $S0$). First, we set $SW1$ into the tuning position and monitor the open-loop output of the lock-in amplifier $S3$ while adjusting the phase ϑ until $S3$ becomes zero. Next, we subtract 90° from ϑ to obtain the maximum feedback signal. Finally, we set $SW1$ back into normal KFM position and monitor the closed-loop

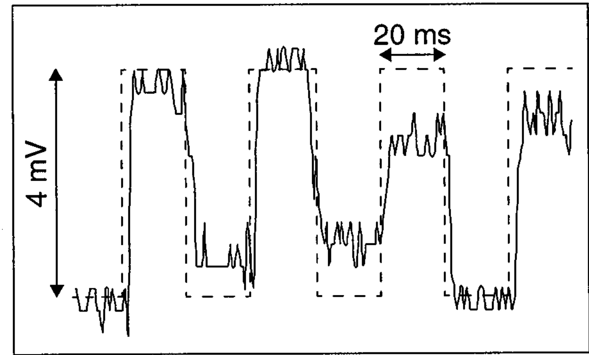

FIG. 6. Accuracy and noise value of the closed-loop dc tip potential $S4$. The potential (solid line), measured locally on template stripped gold (Ref. 17) at a lift height of 20 nm, follows the applied square wave voltage (4 mV_{ptp}, 20 Hz, dashed line) with an accuracy of 1 mV. The measured noise value within a bandwidth of 1 kHz is below 1 mV_{ptp}.

dc tip voltage $S4$ while optimizing the controller gains until $S4$ tracks the external voltage source. Figure 5 displays a series of open-loop lock-in signals $S3$ and the corresponding closed-loop tip voltages $S4$ for different values of $(\varphi-\vartheta)$ as obtained when fine tuning the feedback. The detected open-loop lock-in signal $S3$ ($SW1$ connected to GND, hence $U_{dc}=0$) is proportional to $-Us^*\cos(\varphi-\vartheta)$, and is maximized when the phase difference $(\varphi-\vartheta)$ equals 180°. In closed-loop operation, i.e., normal KFM mode, this phase difference results in $S4$ tracking the external voltage source best. $S4$ is the dc voltage applied to the tip and equal to the local CPD. Operating the feedback at maximum sensitivity ensures that tracking of small changes in the surface potential (<1 mV_{ptp}) becomes possible (Fig. 6).

Nonetheless, one might wonder whether optimization of the feedback loop is not possible based on the appearance of the contact potential image alone. Figure 7 clearly demonstrates that a phase difference $(\varphi-\vartheta)$ off by 45° from the optimum value $[(\varphi-\vartheta)=180°]$ still yields reasonable con-

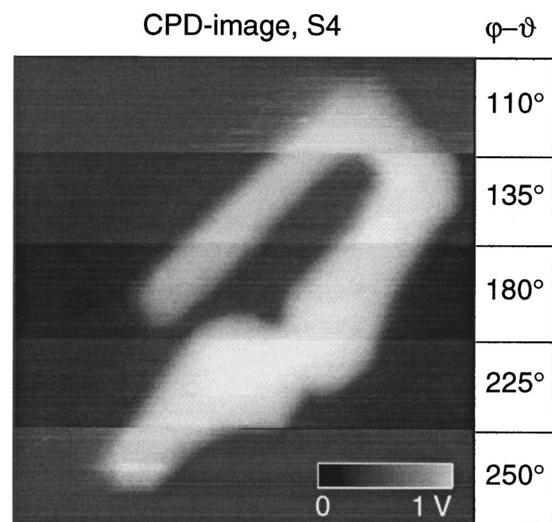

FIG. 7. CPD image of the perforated metal film at different values $(\varphi-\vartheta)$. Even for a phase difference off by 45° from the optimum value reasonable contrast is obtained in the CPD image. Also, the sensitivity of the feedback is reduced by a factor of cos(45°).

Downloaded 20 Jan 2009 to 128.101.170.33. Redistribution subject to AIP license or copyright; see http://rsi.aip.org/rsi/copyright.jsp

trast, making it difficult to judge the optimal setting based on the quality of the contact potential, particularly on samples with unknown features. Therefore, we recommend to fine tune the feedback loop via the procedure described above.

After the phase and the controller gains have been optimized, the feedback loop compensates the CPD, and the ω component of the cantilever deflection becomes approximately zero, resulting in a reduced total cantilever deflection. As a result, the lift height can further be reduced without touching the surface thereby improving spatial resolution[13,14] of the measured potential distribution as can be seen when comparing Fig. 3(e) [lift height 15 nm, $(\varphi-\vartheta)=180°$] with Fig. 7 (lift height 40 nm).

ACKNOWLEDGMENTS

This work was supported by the ETH Zurich and the Swiss National Science Foundation, NRP Nanosciences, Grant No. 4036-044062.

[1] P. Muralt and D. W. Pohl, Appl. Phys. Lett. **48**, 514 (1986).
[2] J. R. Kirtley, S. Washburn, and M. J. Brady, Phys. Rev. Lett. **60**, 1546 (1988).
[3] J. P. Pelz and R. H. Koch, Rev. Sci. Instrum. **60**, 301 (1989).
[4] Y. Martin, D. W. Abraham, and H. K. Wickramasinghe, Appl. Phys. Lett. **52**, 1103 (1988).
[5] M. R. Weaver and D. W. Abraham, J. Vac. Sci. Technol. B **9**, 1559 (1991).
[6] M. Nonnenmacher, M. P. O'Boyle, and H. K. Wickramasinghe, Appl. Phys. Lett. **58**, 2921 (1991).
[7] A. Kikukawa, S. Hosaka, and R. Imura, Appl. Phys. Lett. **66**, 3510 (1995).
[8] M. Yasutake, Jpn. J. Appl. Phys., Part 1 **34**, 3403 (1995).
[9] A. Chavez-Pirson, O. Vatel, M. Tanimoto, H. Ando, H. Iwamura, and H. Kanbe, Appl. Phys. Lett. **67**, 3069 (1995).
[10] M. Arakawa, S. Kishimoto, and T. Mizutani, Jpn. J. Appl. Phys., Part 1 **36**, 1826 (1997).
[11] M. Fujihira and H. Kawate, J. Vac. Sci. Technol. B **12**, 1604 (1994).
[12] S. Yamashina and M. Shigeno, J. Electron. Microsc. **44**, 462 (1995).
[13] H. O. Jacobs, H. F. Knapp, S. Müller, and A. Stemmer, Ultramicroscopy **69**, 39 (1997).
[14] H. O. Jacobs, P. Leuchtmann, O. J. Homan, and A. Stemmer, J. Appl. Phys. **84**, 1168 (1998).
[15] W. Nabhan, B. Equer, A. Broniatowski, and G. De Rosny, Rev. Sci. Instrum. **68**, 3108 (1997).
[16] S. J. O'Shea, R. M. Atta, and M. E. Welland, Rev. Sci. Instrum. **66**, 2508 (1995).
[17] M. Hegner, P. Wagner, and G. Semenza, Surf. Sci. **291**, 39 (1993).

Downloaded 20 Jan 2009 to 128.101.170.33. Redistribution subject to AIP license or copyright; see http://rsi.aip.org/rsi/copyright.jsp